González Sorribes, A.; Cuenca, Á.; Salt Llobregat, JJ.; Jacobs, J. (2021). Robust stability analysis of an energy-efficient control in a Networked Control System with application to Unmanned Ground Vehicles. Information Sciences. 578:64-84. https://doi.org/10.1016/j.ins.2021.07.016

Robust stability analysis of an energy-efficient control in a Networked Control System with application to Unmanned Ground Vehicles[☆]

Antonio González, Ángel Cuenca, Julián Salt, Jelle Jacobs

Abstract

In this paper, the robust stability and disturbance rejection performance analysis of an energy-efficient control is addressed in the framework of Networked Control System (NCS). The control scheme under study integrates periodic event-triggered control, packet-based control, time-varying Kalman filter, dual-rate control and prediction techniques, whose design is aimed at reducing energy consumption and bandwidth usage. The robust stability against time-varying model uncertainties is analyzed by means of a sufficient condition based on Linear Matrix Inequalities (LMI). Finally, the effectiveness of the proposed approach is experimentally validated in a tracking control for an Unmanned Ground Vehicle (UGV), which is a battery-constrained mobile device with limited computation capacities.

Keywords: Energy efficiency, Networked Control System, Dual-rate control, Kalman filter, Unmanned Ground Vehicle

1. Introduction

The research of control synthesis methods for increasing the energy-efficiency of the control system has been a subject of research for the last years

[☆]a) This manuscript is the authors' original work and has not been published nor has it been submitted simultaneously elsewhere. b) All authors have checked the manuscript and have agreed to the submission. The corresponding author is A. González. A. González, A. Cuenca, J. Salt are with the Instituto de Automática e Informática Industrial (AI2), Universitat Politècnica de València (UPV), Spain. (e-mail: angonsor@upv.es,acuenca@isa.upv.es,julian@isa.upv.es). J. Jacobs is with the Department of Mechanical Engineering, Eindhoven University of Technology, Eindhoven (The Netherlands); jelle_jacobs@hotmail.nl

[44, 45]. An appropriate design for efficiently controlling energy-consuming systems is a critical aspect in many control engineering applications, such as heating [39], chemical processes [37], electric vehicles [19], solar energy systems [50], where many of them are implemented in Networked Control Systems (NCS) [2, 31].

NCS are control systems in which the plant to be controlled and the rest of control devices are spatially distributed, and hence, the communication among them occurs through a shared and band-limited digital communication network [47]. Taking into account the limited communication bandwidth, the use of event-triggered control (ETC) for data transmission are advantageous with respect to time-triggered protocols [21, 26], since data packets are only transmitted when certain event conditions are satisfied. This feature has motivated the implementation of ETC approaches into NCS designs under different scenarios, such as the presence of denial-of-service attacks [42, 17], aperiodic sampling schemes [43] and multiagent systems [30, 46], among others. In particular, wireless communication networks are sometimes preferred, especially in a context where it is quite expensive and difficult to install wired connections. However, network devices are usually powered by means of batteries with limited capacity, so wireless data transmission may become very expensive in terms of energy consumption [33]. Hence, achieving a reliable wireless communication through a suitable NCS design aimed at reducing energy waste is crucial in order to maximize network lifetime [1]. In this kind of setups, the benefits of ETC has been discussed not only to save bandwidth resources but also to improve energy efficiency [9, 15, 10].

Another useful solution that contributes to reduce bandwidth and energy consumption in wireless NCS is to employ different rates for sensor and actuator. In this method, known in the literature as dual-rate control [24], measurement data are acquired at slow rate, and control actions are injected at fast rate in order to improve closed-loop performance to some extent (see, e.g., [35]). This kind of control solution, combined with packet-based control strategies (see, e.g., [7]), enables to only send data through the network at the slow rate.

Apart from energy and bandwidth constraints, other negative effects inherent to NCS are time-varying communications delays, packet dropouts and packet disorder. Such phenomena have been widely investigated in the literature. Time-varying delays in the control system has been tackled under different approaches: state-feedback control [6], state estimators [32],

multi-rate control [34] and predictor-feedback control approaches [13]. Further extensions were adapted to deal with time-varying delays together with packet dropouts by gain-scheduling predictor-feedback approaches [14, 15], and active disturbance rejection by integrating an extended state observer [20]. Packet dropouts have also been faced using predictive control [25], gain scheduling [12], and predictor-observer methods [9]. In the latter case, the underlying idea is to reconstruct the actuator and sensor signals by combining predictor approaches with a Luenberger observer. Other alternative observer-based methods resort to proportional multi-integral observers for signal reconstruction in the presence of actuator and sensor faults [23]. Lastly, packet disordering has also been addressed by introducing different packet reordering mechanisms [27, 28], and by means of dual-rate control [34, 8, 7].

Very recently, an energy-efficient control strategy was proposed in [1] applied to an output-feedback tracking control of a UGV in a wireless sensor network. The proposed control scheme combines event-triggered protocols and dual-rate control with the objective of reducing energy and bandwidth consumption. Moreover, a predictor-based observer was integrated with a Time-Varying Dual-Rate Kalman Filter (TVDRKF) in order to deal with packet dropouts and time-varying delays. This work provides simulation results performed by means of a Truetime application [5], showing the achieved improvements in terms of energy efficiency and reduction of bandwidth usage. Nevertheless, to the best of the authors' knowledge, two aspects have been not addressed in previous related works: (i) a formal analysis of the closed-loop control performance in terms of robust stability against model mismatches and disturbance rejection as a function of the event-triggered thresholds, and (ii) an experimental validation of the proposed NCS design. Indeed, demonstrators of ETC implemented in NCS are rare, where some exceptions can be found in [15, 11, 22, 36, 8].

In this paper, the stability analysis is carried out via Lyapunov approaches and robust control theory. As a result, a sufficient condition is obtained to ascertain the robust stability of the closed-loop control system with guaranteed disturbance rejection index in terms of Linear Matrix Inequalities (LMI) [4], which can be efficiently solved using available semidefinite programming tools. Moreover, experimental data is also provided to validate the effectiveness of the control design in a prototype consisting in a UGV, which is a two-wheel Lego Mindstorms EV3 robot equipped with a wifi-dongle to send and receive data-packages through the wireless network.

The paper is structured as follows: Section 2 describes the problem state-

ment and gives some preliminaries. Section 3 introduces the proposed control strategy. Section 4 addresses the robust stability analysis of the closed-loop system. Section 5 presents the application of the control solution to a UGV, studying the robust stability of the control system, and providing simulation results and their experimental validation. Finally, some conclusions are gathered in Section 6.

2. Problem statement and preliminaries

Let $G_p(s)$ be the transfer function of the plant system to be controlled. A discrete-time state-space representation of the discretized system $G_p(s)$ with zero-order hold (ZOH) at sampling period T considering model uncertainties yields:

$$\begin{aligned} x_{p,k+1}^T &= (A_p + \Delta_{A,k})\, x_{p,k}^T + (B_p + \Delta_{B,k}) \left(u_k^T + d_k^T\right), \\ y_k^T &= C_p x_{p,k}^T + v_k^T \end{aligned} \tag{1}$$

where $x_{p,k}^T \in \mathcal{R}^{n_p}$ is the state vector containing n_p state variables of the plant system, $u_k^T \in \mathcal{R}^m$ is the control input with m input signals, $d_k^T \in \mathcal{R}^m$ is a matched disturbance input (assumed to be unmeasurable), $y_k^T \in \mathcal{R}^q$ represents the output system with q output signals, $v_k^T \in \mathcal{R}^q$ is the measurement noise, A_p, B_p, C_p are the state-space matrices of appropriate dimensions, and $\Delta_{A,k}, \Delta_{B,k}$ are time-varying model uncertainties described below in (4).

In this paper, dual-rate control is used in the controller scheme with two different periods: T as the actuation period, and NT as the sensing period, being $N \in \mathbb{N}^+$ the multiplicity between the two periods of the dual-rate control scheme. Thereafter, let us respectively introduce the notation $(.)_k^T$ and $(.)_k^{NT}$ to denote a T-period and an NT-period signal or variable, where $k \in \mathbb{N}$ are iterations at the corresponding period.

Consider the NCS described in Fig. 1, where two main components can be distinguished: local side and remote side. The local side includes the sensor, actuator, and the plant system $G_p(s)$ to be controlled. As computational resource constraints are assumed at the local side, the digital control algorithm is located in a computationally powerful device at the remote side. Remote and local sides are connected by a shared communication network, where communication delays and packet dropouts may occur. For a packet sampled at instant kNT, being effectively sent (i.e., the trigger conditions hold)

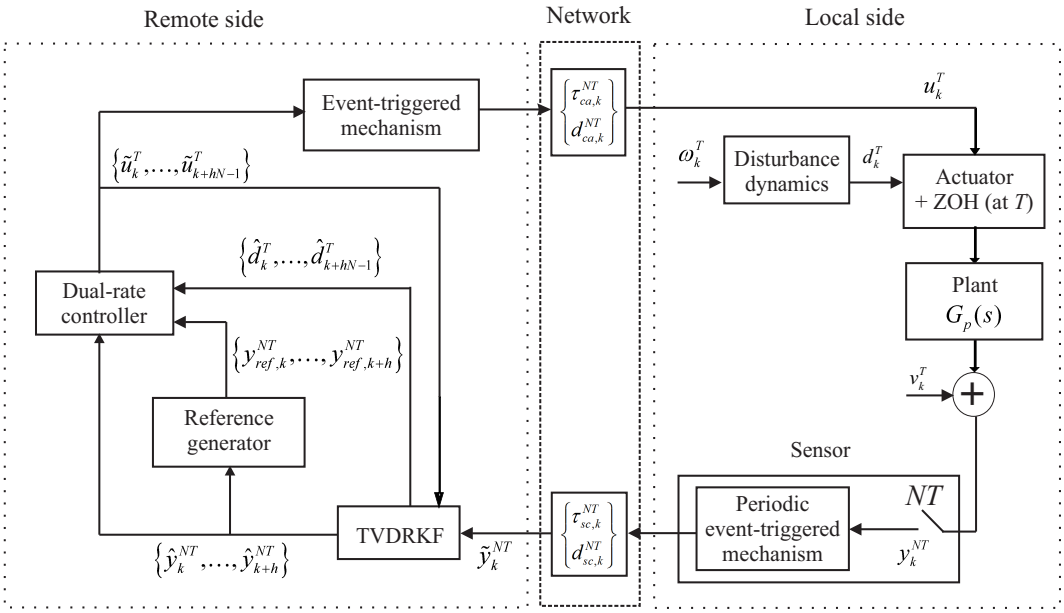

Figure 1: Proposed control scheme for the NCS

and not lost, the round-trip time delay is defined as $\tau_k^{NT} = \tau_{ca,k}^{NT} + \tau_{sc,k}^{NT} + \tau_{c,k}$, where $\tau_{ca,k}^{NT}$ and $\tau_{sc,k}^{NT}$ are the communication delay induced by the controller-to-actuator and sensor-to-controller channels, respectively, and $\tau_{c,k}$ is a computation time delay. Packet dropouts are contemplated as a Bernoulli process, whose probability of dropout is respectively given by p_{sc} and p_{ca}:

$$\begin{aligned} p_{sc} &= \Pr[d_{sc,k}^{NT} = 0] \in [0,1) \\ p_{ca} &= \Pr[d_{ca,k}^{NT} = 0] \in [0,1) \end{aligned} \tag{2}$$

The structure of the output predictor-feedback control u_k^T is designed with the objective of reducing energy and bandwidth consumption. For this purpose, a periodic event-triggered control is combined with packet-based control, time-varying dual-rate Kalman filter, prediction techniques, and dual-rate control. A detailed description is later presented in Section 3.

The objective of this paper is two-fold: (i) to provide sufficient conditions to ascertain the robust stability of the designed NCS with guaranteed disturbance rejection index, and (ii) validate the control strategy in an experimental setup consisting in a tracking control of a UGV.

The following assumptions and preliminary results are given for the stability analysis and control synthesis:

Assumption 1. *The disturbance $d_k^T \in \mathcal{R}^m$ can be modeled by the following exogenous system [20]:*

$$\begin{aligned} x_{d,k+1}^T &= A_d x_{d,k}^T + B_d \omega_k^T, \\ d_k^T &= C_d x_{d,k}^T \end{aligned} \tag{3}$$

where $A_d \in \mathcal{R}^{r\times r}$, $B_d \in \mathcal{R}^{r\times m}$, $C_d \in \mathcal{R}^{m\times r}$ are known matrices, the initial conditions $x_{d,0}$ is assumed to be unknown, and $\omega_k \in \mathcal{R}^q$ represents an unknown disturbance component. This assumption allows modeling some specific type of disturbances typically encountered in many industrial applications, such as harmonics or unknown load disturbances [16].

Assumption 2. *Time-varying model uncertainties are assumed to be described as a norm-bounded form [18]:*

$$(\Delta_{A,k}, \Delta_{B,k}) = \delta_\Delta E_p \Delta_k \left(H_{p,A}, H_{p,B}\right) \tag{4}$$

where $\delta_\Delta \geq 0$ is a scalar that determines the size of uncertainties, $\Delta_k \in \mathcal{R}^{l_1\times l_2}$ represents any unknown time-varying matrix satisfying $\Delta_k^{'}\Delta_k \leq I, \forall k \geq 0$, where hereinafter the notation $(\cdot)^{'}$ denotes the transpose function, and $E_p \in \mathcal{R}^{n_p\times l_1}$, $H_{p,A} \in \mathcal{R}^{l_2\times n_p}$, $H_{p,B} \in \mathcal{R}^{l_2\times m}$ are time-constant matrices that define the structure of such uncertainties. The norm-bounded form (4) can be understood as an ellipsoid around the nominal state-space matrices whose shape is defined through matrices $E_p, H_{p,A}, H_{p,B}$, and whose size is determined by the scalar δ_Δ. This model is widely used in the literature to describe uncertain systems with time-varying model mismatches, and may include parametric uncertainties, unmodeled dynamics, small variations in the sampling period [40] and in general all possible source of bounded uncertainties. Note that (4) can also describe unmatched disturbances by choosing, for instance, $E_p = diag\left(E_{p1}, E_{p2}\right)$ and $\Delta_k = (\Delta_{1,k}, \Delta_{2,k})$ with uncorrelated time-varying matrices $\Delta_{1,k}$, $\Delta_{2,k}$. In this case, $\Delta_{A,k}$ and $\Delta_{B,k}$ are not necessarily in the same range space as the nominal input matrix B_p [43].

Remark 1. *The sampling period at slow rate is chosen to be larger than the largest round-trip time delay $\tau_{max} = max\left(\tau_k^{NT}\right), \forall k \geq 0$ in order to avoid packet disorder, that is to say, $NT > \tau_{max}, \forall k \geq 0$. The largest round-trip delay can be available by assuming prior knowledge of a statistical distribution for the network-induced delay [3].*

Remark 2. *System* $x_{k+1}^{NT} = Ax_k^{NT} + Bu_k^{NT}$, $y_k^{NT} = Cx_k^{NT}$ *with* $A \in \mathcal{R}^n$, $B \in \mathcal{R}^{n\times m}$ *and* $C \in \mathcal{R}^{q\times n}$ *can equivalently be written at fast period* T *as* $x_{k+N}^T = Ax_k^T + Bu_k^T$, $y_k^T = Cx_k^T$, *and in augmented form at fast period as:*

$$\begin{aligned} \bar{x}_{k+1}^T &= \bar{A}\bar{x}_k^T + \bar{B}u_k^T, \\ y_k^T &= \bar{C}\bar{x}_k^T \end{aligned} \tag{5}$$

where $\bar{x}_k^T = \begin{bmatrix} \left(x_{k-1}^T\right)' & \left(x_{k-2}^T\right)' & \cdots & \left(x_{k-N}^T\right)' \end{bmatrix}'$ *and*

$$\bar{A} = \begin{bmatrix} 0 & A \\ I_{(N-1)n} & 0 \end{bmatrix}, \ \bar{B} = \begin{bmatrix} B \\ 0_{(N-1)n\times m} \end{bmatrix}, \ \bar{C} = \begin{bmatrix} 0_{q\times(N-1)n} & C \end{bmatrix} \tag{6}$$

3. Proposed control scheme

This section presents the proposed control system (see Figure 1). Both in remote and local sides, event-triggered protocols are designed in order to decide when the data must be sent through the network. A detailed description of each component of the control scheme is provided in the next subsections.

3.1. Event-triggered protocol for transmission of measurement data

The measurements of the output system y_k^T are sent from sensors next to the plant system to the controller via network at slow period NT under the following event-triggered mechanism:

$$\tilde{y}_k^{NT} = \begin{cases} y_k^{NT} & \text{if (8) is true} \\ \tilde{y}_{k-1}^{NT} & \text{otherwise} \end{cases} \tag{7}$$

The measurement y_k^{NT} is therefore transmitted if the following event-triggered condition periodically evaluated at period NT is satisfied:

$$(y_k^{NT} - \tilde{y}_{k-1}^{NT})'\Omega_y(y_k^{NT} - \tilde{y}_{k-1}^{NT}) > \sigma_y^2 \left(y_k^{NT}\right)' \Omega_y y_k^{NT} + \delta_y, \tag{8}$$

where $\Omega_y \in \mathcal{R}^p > 0$, and $\sigma_y, \delta_y \in \mathcal{R} \geq 0$ are event-triggered parameters that define the threshold level to decide whether the measurement data packet must be sent or not to remote side.

3.2. Event-triggered protocol for transmission of control actions

Taking into account (7) and (8), the outputs sampled at the slow rate $1/NT$ may arrive at the remote side at a slower rate $1/\bar{N}T$ in a non-uniform fashion. Let $\mu = \bar{N}/N$, where μ is the number of consecutive packet dropouts. Note that both μ and $\bar{N}$ will be time-varying due to the non-uniform nature of the time sampling pattern. Consider the mixed event-triggered protocol to decide when the set of control actions $\{\tilde{u}_k^T,\ \tilde{u}_{k+1}^T,\ ...,\ \tilde{u}_{k+hN-1}^T\}$ must be transmitted via network from the controller to the actuator, where $\tilde{u}_k^T$ is defined in (31), and $h = max(\mu)$ is the maximum number of consecutive packet dropouts. The above set of control actions is transmitted if the following event-triggered condition is satisfied for the first control action:

$$(\tilde{u}_k^T - u_{k-1}^T)'\Omega_u(\tilde{u}_k^T - u_{k-1}^T) > \sigma_u^2 \left(\tilde{u}_k^T\right)' \Omega_u \tilde{u}_k^T + \delta_u, \tag{9}$$

where (9) is evaluated each time a new output measurement is received (i.e., when (8) is satisfied), and $\Omega_u \in \mathcal{R}^m > 0$, and $\sigma_u, \delta_u \in \mathcal{R} \geq 0$ are event-triggered parameters that define the threshold level to decide whether the data packet containing the set of control actions must be sent or not to local side. Then, we have that:

$$u_k^T = \begin{cases} \tilde{u}_k^T & \text{if (9) is true} \\ u_{k-1}^T & \text{otherwise} \end{cases} \tag{10}$$

3.3. Time-Varying Dual-Rate Kalman Filter (TVDRKF)

Let $x_k^T = \left[\left(x_{p,k}^T\right)' \quad \left(x_{d,k}^T\right)'\right]'$. From (1) and (3), an augmented state-space model can be obtained as:

$$\begin{aligned} x_{k+1}^T &= A_k x_k^T + B_k u_k^T + B_\omega \omega_k^T, \\ y_k^T &= C x_k^T + v_k^T, \\ d_k^T &= \mathcal{C}_d x_k^T \end{aligned} \tag{11}$$

where $A_k = A + \delta_\Delta E \Delta_k H_A$, $B_k = B + \delta_\Delta E \Delta_k H_{p,B}$, and

$$A = \begin{bmatrix} A_p & B_p C_d \\ 0 & A_d \end{bmatrix}, \quad B = \begin{bmatrix} B_p \\ 0 \end{bmatrix}, \quad B_\omega = \begin{bmatrix} 0 \\ B_d \end{bmatrix}, \ C = \begin{bmatrix} C_p & 0 \end{bmatrix}, \tag{12}$$
$$\mathcal{C}_d = \begin{bmatrix} 0 & C_d \end{bmatrix}, \quad E = \begin{bmatrix} E_p \\ 0 \end{bmatrix}, \quad H_A = \begin{bmatrix} H_{p,A} & 0 \end{bmatrix},$$

The best linear estimation for x_k^T in the sense of mean square error is obtained by means of the conventional Kalman filter [38] by considering ω_k^T and v_k^T as zero-mean white noises for system (11). In case of having different rates in the control system, a multi-rate Kalman filter containing corrections and predictions is necessary [49]. In the proposed control scheme, a dual-rate control and periodic ETC are implemented with the objective of minimizing bandwidth and energy consumption. Consequently, some measurements are not sent to the remote side, leading to a Time-Varying Dual Rate Kalman Filter (TVDRKF) [41, 9].

In addition, from extended state observer [48] and multi-rate Kalman filter [49] methods, the proposed TVDRKF is able to estimate the plant measurement and disturbance by implementing the augmented system model given in (11).

Let $\hat{x}_{k|k}^T$ the estimation of the system state x_k^T defined in (11). When the output measurement $\tilde{y}_k^{NT}$ (see (7)) is available at the remote side, the TVDRKF can perform the correction (and filtering) stage:

$$\hat{x}_{k|k}^T = \hat{x}_{k|k-\bar{N}}^T + K(\bar{N})\left(\tilde{y}_k^T - C\hat{x}_{k|k-\bar{N}}^T\right) \tag{13}$$

where $\hat{x}_{k|k-\bar{N}}^T$ is the current prediction, which was obtained by iterating the prediction formula given below (14) $\bar{N}$ steps ahead from the estimation made at instant $(k-\bar{N})T$. When no measurement data is received, the above state estimation is updated at fast rate T using (14) for $l = 1, 2, .., \bar{N}_{max}$ with $\bar{N}_{max} = hN$.

$$\hat{x}_{k+l|k}^T = A^l \hat{x}_{k|k}^T + \sum_{c=0}^{l-1} A^{l-1-c} B \tilde{u}_{k+c}^T \tag{14}$$

The time-varying $K(\bar{N})$ can be calculated by multi-rate Kalman filter design techniques as

$$\begin{aligned} K(\bar{N}) &= M_{k+1}C'[CM_{k+1}C' + V]^{-1} \\ M_{k+1} &= A^{\bar{N}} M_k (A^{\bar{N}})' + W_e - A^{\bar{N}} M_k C'[CM_k C' + V]^{-1} C M_k (A^{\bar{N}})' \end{aligned} \tag{15}$$

where matrices A, B, C are given in (12), $V = Cov(v_k^T)$ being v_k^T the mea-

surement noise, and

$$\begin{aligned} W_e &= Cov\left(\sum_{c=0}^{\bar{N}-1} A^{\bar{N}-1-c} B_\omega \omega_{k+c}^T\right) \\ &= \mathcal{E}\left\{\left(\sum_{c=0}^{\bar{N}-1} A^{\bar{N}-1-c} B_\omega \omega_{k+c}^T\right)\left(\sum_{c=0}^{\bar{N}-1} A^{\bar{N}-1-c} B_\omega \omega_{k+c}^T\right)'\right\} \end{aligned} \tag{16}$$

where $\mathcal{E}\{\cdot\}$ denotes the expectation. The process noise ω_k^T is assumed to be uncorrelated, i.e., $\mathcal{E}\left(\omega_{k+c}^T \omega_k^{T'}\right) = 0,\ \forall c \neq 0$. Hence, from (16) it can be deduced that

$$W_e = \sum_{c=0}^{\bar{N}-1} \left(A^{\bar{N}-1-c} B_\omega\right) W \left(A^{\bar{N}-1-c} B_\omega\right)' \tag{17}$$

where $W = Cov(\omega_k^T)$, being ω_k^T the process noise.

Moreover, from (14), the set of hN estimated outputs and disturbances can be calculated as follows:

$$\begin{aligned} \hat{y}_{k+l}^T &= C\hat{x}_{(k+l|k)}^T \\ \hat{d}_{k+l}^T &= \mathcal{C}_d \hat{x}_{(k+l|k)}^T \end{aligned} \tag{18}$$

Figure 2 summarizes the structure of the TVDRKF.

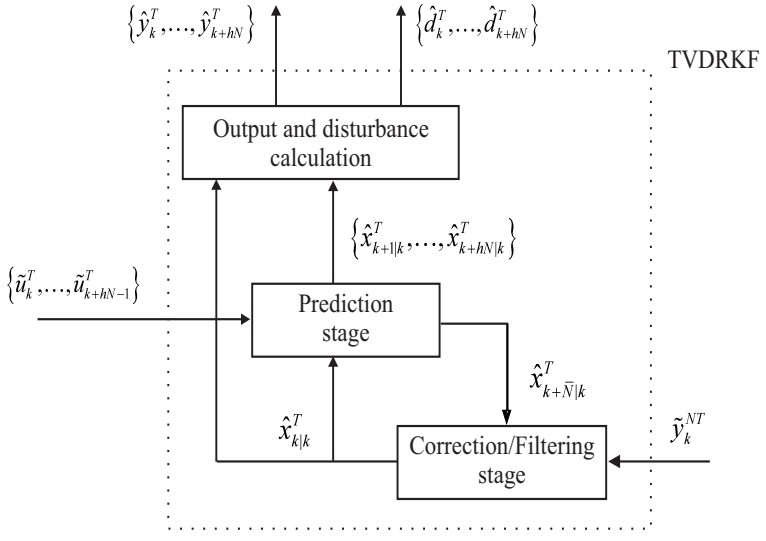

Figure 2: Structure of the Time-Varying Dual-Rate Kalman Filter

3.4. Dual-rate controller:

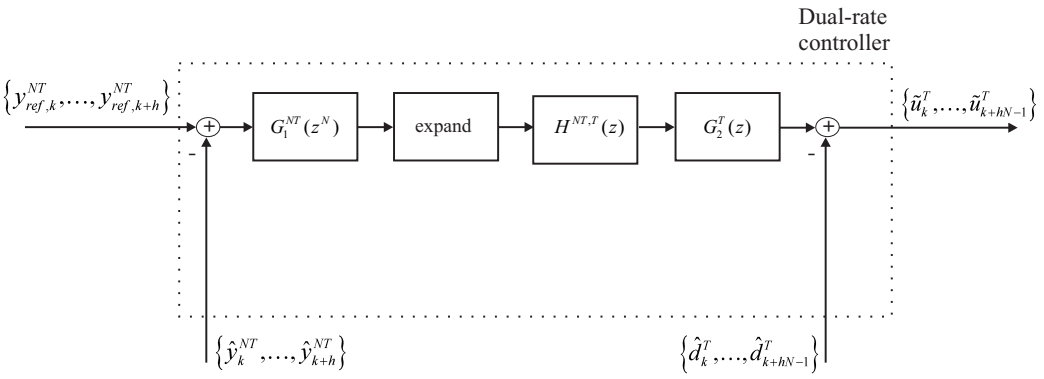

Figure 3: Dual-rate controller scheme

In this work we design a model-based dual-rate controller [35]. Using Z-transform at period T, the dual-rate control structure is defined as follows (see Fig. 3):

- a slow-rate subcontroller $G_1^{NT}(z^N) = u_{1,k}^{NT}/e_k^{NT}$,
- a digital hold $H^{NT,T}(z) = u_{1,k}^T/[u_{1,k}^{NT}]^T$, and
- a fast-rate subcontroller $G_2^T(z) = \tilde{u}_{2,k}^T/u_{1,k}^T$.

where z is the T-unit operator. The input of $G_1^{NT}(z^N)$ is the tracking error $e_k^{NT} = y_{ref,k}^{NT} - \hat{y}_k^{NT}$, being $y_{ref,k}^{NT}$ the output tracking reference and $\hat{y}_k^{NT}$ the estimation of the output system obtained by the TVDRKF explained in Section 3.3.

The dynamic dual-rate controller computes N control actions at period T, which can be arranged in the augmented vector:

$$\{\tilde{u}_{2,k}^T, \tilde{u}_{2,k+1}^T, \ldots, \tilde{u}_{2,k+N-1}^T\}.$$

The anti-disturbance approach is implemented by finally subtracting the disturbance estimations generated by the TVDRKF at period T,

$$\{\hat{d}_k^T, \hat{d}_{k+1}^T, \ldots, \hat{d}_{k+N-1}^T\},$$

which are obtained from (18), leading to $\{\tilde{u}_k^T, \tilde{u}_{k+1}^T, \ldots, \tilde{u}_{k+N-1}^T\}$, where $\tilde{u}_{k+l}^T = \tilde{u}_{2,k+l}^T - \hat{d}_{k+l}^T$ with $l = 0, 1, ..., N-1$. Following this operation mode for the next

h dynamic references and outputs, $\{\hat{y}^{NT}_{ref,k+1}, \ldots, \hat{y}^{NT}_{ref,k+h}\}$ and $\{\hat{y}^{NT}_{k+1}, \ldots, \hat{y}^{NT}_{k+h}\}$, respectively, and the next hN disturbances $\{\hat{d}^{T}_{k+N}, \ldots, \hat{d}^{T}_{k+hN-1}\}$, the set of future control actions $\{\hat{u}^{T}_{k+N}, \ldots, \hat{u}^{T}_{k+hN-1}\}$ can be obtained.

Notice that the output of $G^{NT}_1(z^N)$ (i.e, $u^{NT}_{1,k}$) is expanded $[u^{NT}_{1,k}]^T$ before being injected to the digital hold $H^{NT,T}(z)$. The expand operation implies to fill the slow-rate signal with zeros at the fast-rate instants (more details can be found in [35]).

The digital hold $H^{NT,T}(z)$ retains the last injected value of the slow-rate controller output signal $u^{NT}_{1,k}$, which implies that the sub-controller output $u^{NT}_{1,k}$ is repeated N times. Hence, the transfer function of the digital hold can be expressed as:

$$H^{NT,T}(z) = \frac{1 - z^{-N}}{1 - z^{-1}}$$

The dual-rate control design method can be performed from the desired transfer function of the continuous-time closed-loop system $M(s)$. Let us consider $M^T(z)$ and $M^{NT}(z^N)$ as the ZOH-based discretization of $M(s)$ at two different sampling periods: T and NT, respectively. Then, the subcontrollers $G^{NT}_1(z^N)$ and $G^T_2(z)$ will be designed as follows [35]:

$$G^{NT}_1(z^N) = \frac{1}{1 - M^{NT}(z^N)} \tag{19}$$

and

$$G^T_2(z) = \frac{M^T(z)}{G^T_p(z)} \tag{20}$$

where $G^T_p(z) = C_p\,(zI - A_p)^{-1}\,B_p$ is the discrete-time transfer function of the nominal system (1) at period T under ZOH conditions.

4. Stability analysis

Before proceeding with the stability analysis, an equivalent interconnected state-space representation of the closed-loop system (1) and the proposed NCS in Section 3 is obtained through Section 4.1 and 4.2. The closed-loop model (33) allows us to further address the stability analysis in the framework of LMI via Lyapunov method in Section 4.3.

4.1. State-space description

Since each device operates at a different period, the plant model and the different components of the control system presented in Section 3 are first converted at fast rate using lifting techniques. In this way, an equivalent interconnected representation for the closed-loop system is found in (33) by including the above defined event-triggered protocols and time-varying model uncertainties. For this purpose, input/output approaches have been suitably applied to embed them into a single norm-bounded uncertain system (namely Δ in (33)). Next subsections give a detailed description of how each subsystem model has been obtained to further integrate them into (33).

4.1.1. Plant model

To deal with the event-triggered protocol for transmission of control actions defined in Section 3.2 and model uncertainties (4), let us define the following new inputs:

$$\begin{aligned} \rho_{u,k}^T &= u_k^T - \tilde{u}_k^T, \\ w_{\Delta,k}^T &= \Delta_k y_{\Delta,k}^T \end{aligned} \tag{21}$$

where $y_{\Delta,k}^T = H_A x_k^T + H_{p,B} u_k^T$.

From the above definition and (4), we have that $u_k^T = \tilde{u}_k^T + \rho_{u,k}^T$ and $\Delta_{A,k} + \Delta_{B,k} = E w_{\Delta,k}^T$. Then, (11) can be rewritten as the interconnected system:

$$\begin{aligned} x_{k+1}^T &= A x_k^T + B\tilde{u}_k^T + B\rho_{u,k}^T + B_\omega \omega_k^T + \delta_\Delta E w_{\Delta,k}^T, \\ y_{\Delta,k}^T &= H_A x_k^T + H_{p,B}\tilde{u}_k^T + H_{p,B}\rho_{u,k}^T, \\ y_k^T &= C x_k^T + v_k^T \end{aligned} \tag{22}$$

where $w_{\Delta,k}^T = \Delta_k y_{\Delta,k}^T$.

4.1.2. Time-Varying Dual-Rate Kalman Filter

To cope with the event-triggered protocol for transmission of measurement data defined in Section 3.1, let us introduce the following input:

$$\rho_{y,k}^{NT} = \tilde{y}_k^{NT} - y_k^{NT} \tag{23}$$

From the above definition, we have that $\tilde{y}_k^{NT} = y_k^{NT} + \rho_{y,k}^{NT}$. The TVDRKF (13) and (14) can be expressed in augmented form at fast period T as:

$$\bar{\tilde{x}}_{k+1}^T = \mathcal{A}_{\bar{N}} \bar{\tilde{x}}_k^T + \mathcal{B}_{\bar{N}} \bar{\tilde{u}}_k^T + \left(\mathcal{K}_{\bar{N}} C\right) x_k^T + \left(\mathcal{K}_{\bar{N}} C\right) \rho_{y,k}^T + \mathcal{K}_{\bar{N}} v_k^T \tag{24}$$

where

$$\bar{\hat{x}}_{k+1}^T = \left[\left(\hat{x}_{k|k}^T\right)' \quad \left(\hat{x}_{k-1|k-\bar{N}}^T\right)' \quad \cdots \quad \left(\hat{x}_{k-\bar{N}+1|k-\bar{N}}^T\right)'\right]', \tag{25}$$

$$\bar{\hat{x}}_k^T = \left[\left(\hat{x}_{k-1|k-\bar{N}}^T\right)' \quad \cdots \quad \left(\hat{x}_{k-\bar{N}|k-\bar{N}}^T\right)'\right]',$$

$$\bar{\tilde{u}}_k^T = \left[\left(\tilde{u}_{k-1}^T\right)' \quad \left(\tilde{u}_{k-2}^T\right)' \quad \cdots \quad \left(\tilde{u}_{k-\bar{N}}^T\right)'\right]',$$

and

$$\mathcal{A}_{\bar{N}} = \begin{bmatrix} 0_n & 0 & A^{\bar{N}} - K(\bar{N})CA^{\bar{N}} \\ I_n & 0 & 0 \\ 0 & I_{(\bar{N}-2)n} & 0_{(\bar{N}-2)n\times n} \end{bmatrix}, \tag{26}$$

$$\mathcal{B}_{\bar{N}} = \begin{bmatrix} B_{\bar{N}} \\ 0_{(\bar{N}-1)n\times \bar{N}m} \end{bmatrix},$$

$$B_{\bar{N}} = \begin{bmatrix} B & AB & \cdots & A^{\bar{N}-1}B \end{bmatrix},$$

$$\mathcal{K}_{\bar{N}} = \begin{bmatrix} K'(\bar{N}) & 0_{q\times(\bar{N}-1)n} \end{bmatrix}',$$

where $n = n_p + r$

4.1.3. Slow-rate controller

The state-space model of the slow-rate controller $G_1^{NT}(z^N)$ can be expressed as:

$$\begin{aligned} \xi_{k+1}^{NT} &= A_\xi \xi_k^{NT} + B_\xi e_k^{NT}, \\ u_{1,k}^{NT} &= C_\xi \xi_k^{NT} + D_\xi e_k^{NT} \end{aligned} \tag{27}$$

where $e_k^{NT} = y_{ref,k}^{NT} - \hat{y}_k^{NT}$, $\hat{y}_k^{NT} = C\hat{x}_{k|k}^{NT}$, $\xi_k \in \mathcal{R}^{n_\xi}$ is the state vector of the slow-rate controller, and $A_\xi \in \mathcal{R}^{n_\xi \times n_\xi}$, $B_\xi \in \mathcal{R}^{n_\xi \times q}$, $C_\xi \in \mathcal{R}^{q_\xi \times n_\xi}$, $D_\xi \in \mathcal{R}^{q_\xi \times q}$ are state-space matrices satisfying $G_1^{NT}(z) = C_\xi \left(zI - A_\xi\right)^{-1} B_\xi + D_\xi$.

From the expand operator it can be deduced that $C_\xi \xi_k^{NT} = \bar{C}_\xi \bar{\xi}_k^T$, where $\bar{C}_\xi = \begin{bmatrix} 0 & C_\xi \end{bmatrix}$ and

$$\bar{\xi}_k^T = \left[\left(\xi_{k-1}^T\right)' \quad \left(\xi_{k-2}^T\right)' \quad \cdots \quad \left(\xi_{k-N}^T\right)'\right]'. \tag{28}$$

Applying Remark 2, the slow-rate controller together with the expand operator can equivalently be represented at fast period T as:

$$\begin{aligned} \bar{\xi}_{k+N}^T &= \bar{A}_\xi \bar{\xi}_k^T + \bar{B}_\xi e_k^T, \\ u_{1,k}^T &= \bar{C}_\xi \bar{\xi}_k^T + D_\xi e_k^T \end{aligned} \tag{29}$$

where

$$\bar{A}_\xi = \begin{bmatrix} 0 & A_\xi \\ I_{(N-1)n_\xi} & 0 \end{bmatrix}, \quad \bar{B}_\xi = \begin{bmatrix} B_\xi \\ 0 \end{bmatrix} \tag{30}$$

4.1.4. Fast-rate controller:

The state-space model of the fast-rate controller $G_2^T(z)$ with anti-disturbance can be expressed as:

$$\begin{aligned} \eta_{k+1}^T &= A_\eta \eta_k^T + B_\eta u_{1,k}^T, \\ \tilde{u}_k^T &= C_\eta \eta_k^T + D_\eta u_{1,k}^T - \hat{d}_k^T \end{aligned} \tag{31}$$

where $u_{1,k}^T$ is the input of the fast-rate controller, $\eta_k \in \mathcal{R}^{n_\eta}$ is the state vector of the fast-rate controller and $A_\eta \in \mathcal{R}^{n_\eta \times n_\eta}$, $B_\eta \in \mathcal{R}^{n_\eta \times q_\xi}$, $C_\eta \in \mathcal{R}^{m \times n_\eta}$, $D_\eta \in \mathcal{R}^{m \times q_\xi}$ are state-space matrices satisfying $G_2^T(z) = C_\eta \left(zI - A_\eta\right)^{-1} B_\eta + D_\eta$.

4.2. Closed-loop system

Recalling the definition of tracking error $e_k^{NT} = y_{ref,k}^{NT} - \hat{y}_k^{NT}$ and the definition of $\bar{\hat{x}}_k^{NT}$ in (25), we have that

$$\bar{e}_k^{NT} = \bar{y}_{ref,k}^{NT} - \bar{C}_y \bar{\hat{x}}_k^{NT} \tag{32}$$

where $\bar{y}_{ref,k}^{NT} = \left[\left(y_{ref,k-1}^{NT}\right)' \quad \cdots, \left(y_{ref,k-h}^{NT}\right)'\right]'$ and $\bar{C}_y = \begin{bmatrix} C & 0_{q \times (\bar{N}-1)n} \end{bmatrix}$.

Hence, from (22), (24), (29), (31) and (32), together with the model uncertainties given in (4), the closed-loop control system can be represented as the interconnected system at period T:

$$\begin{aligned} \mathcal{S}: & \begin{cases} \bar{\phi}_{k+1}^T = A_\phi \bar{\phi}_k^T + B_\phi \bar{\rho}_k^T + B_{\omega,\phi} \bar{\omega}_k^T + \delta_\Delta E_\phi w_{\Delta,k}^T + B_{ref,\phi} \bar{y}_{ref,k}^T \\ y_{\Delta,k}^T = H_\phi \bar{\phi}_k^T + H_{p,B} \bar{\rho}_k^T \\ y_k^T = C_{y,\phi} \bar{\phi}_k^T + C_{\omega,\phi} \bar{\omega}_k^T \end{cases}, \\ \Delta: & \left\{ w_{\Delta,k}^T = \Delta_k y_{\Delta,k}^T \right. \end{aligned} \tag{33}$$

where

$$\begin{aligned}
\bar{\phi}_k^T &= \left[\left(x_k^T\right)' \quad \left(\bar{\tilde{u}}_k^T\right)' \quad \left(\bar{\hat{x}}_k^T\right)' \quad \left(\bar{\xi}_k^T\right)' \quad \left(\eta_k^T\right)' \right]', \\
\bar{\rho}_k^T &= \left[\left(\rho_{u,k}^T\right)' \quad \left(\rho_{y,k}^T\right)' \right]', \\
\bar{\omega}_k^T &= \left[\left(\omega_k^T\right)' \quad \left(v_k^T\right)' \right]'
\end{aligned} \tag{34}$$

$$A_\phi = \begin{bmatrix} A & 0 & -BD_\eta D_\xi \bar{C}_y - B\bar{\mathcal{C}}_d & BD_\eta \bar{C}_\xi & BC_\eta \\ 0 & \Gamma_1 & \Gamma_2 & \Gamma_3 & \Gamma_4 \\ \mathcal{K}_{\bar{N}} C & (\mathcal{B}_{\bar{N}} - \mathcal{K}_{\bar{N}} C B_{\bar{N}}) & \mathcal{A}_{\bar{N}} & 0 & 0 \\ 0 & 0 & -\bar{B}_\xi \bar{C}_y & \bar{A}_\xi & 0 \\ 0 & 0 & -B_\eta D_\xi \bar{C}_y & B_\eta \bar{C}_\xi & A_\eta \end{bmatrix}, \tag{35}$$

$$B_\phi = \begin{bmatrix} B & 0 \\ 0 & 0 \\ 0 & \mathcal{K}_{\bar{N}} \mathcal{C}_{\bar{N}} \\ 0 & 0 \\ 0 & 0 \end{bmatrix}, \quad B_{ref,\phi} = \begin{bmatrix} BD_\eta D_\xi \\ \Gamma_5 \\ 0 \\ \bar{B}_\xi \\ B_\eta D_\xi \end{bmatrix}, \; B_{\omega,\phi} = \begin{bmatrix} B_\omega & 0 \\ 0 & 0 \\ 0 & 0 \\ 0 & 0 \\ 0 & 0 \end{bmatrix} \; E_\phi = \begin{bmatrix} E \\ 0 \\ 0 \\ 0 \\ 0 \end{bmatrix},$$

$$C_{y,\phi} = \begin{bmatrix} C & 0 & 0 & 0 & 0 \end{bmatrix},$$

$$\bar{\mathcal{C}}_d = \begin{bmatrix} \mathcal{C}_d & 0 & 0 & 0 & 0 \end{bmatrix},$$

$$C_{\omega,\phi} = \begin{bmatrix} 0_q & I_q \end{bmatrix},$$

$$H_\phi = \begin{bmatrix} H_A & 0_{l_2 \times \bar{N}m} & -H_{p,B} D_\eta D_\xi \bar{C}_y & H_{p,B} D_\eta \bar{C}_\xi & H_{p,B} C_\eta \end{bmatrix},$$

and

$$\begin{aligned}
\Gamma_1 &= \begin{bmatrix} 0 & 0 \\ I_{(\bar{N}-1)m} & 0 \end{bmatrix}, \qquad \Gamma_2 = \begin{bmatrix} -D_\eta D_\xi \bar{C}_y - \bar{\mathcal{C}}_d \\ 0_{(\bar{N}-1)m \times \bar{N}n} \end{bmatrix}, \\
\Gamma_3 &= \begin{bmatrix} D_\eta \bar{C}_\xi \\ 0_{(\bar{N}-1)m \times N n_\xi} \end{bmatrix}, \qquad \Gamma_4 = \begin{bmatrix} C_\eta \\ 0_{(\bar{N}-1)m \times n_\eta} \end{bmatrix}, \qquad \Gamma_5 = \begin{bmatrix} D_\eta D_\xi \\ 0_{(\bar{N}-1)m \times q} \end{bmatrix}
\end{aligned} \tag{36}$$

4.3. Robust stability analysis of the proposed NCS design

This section gives a sufficient condition to ascertain the robust stability of the closed-loop control system (33) against time-varying model uncertainties (4).

Theorem 1. *Given scalars $\sigma_u, \sigma_y \geq 0$, system (33) is robustly stable if there exist symmetric matrices $P \in \mathcal{R}^{\bar{n}}, \Omega_u \in \mathcal{R}^m, \Omega_y \in \mathcal{R}^q > 0$ with $\bar{n} = n + hN(m+n) + Nn_\xi + n_\eta$ and a scalar $\varepsilon > 0$ such that the following LMI holds:*

$$\begin{bmatrix} -P & 0 & 0 & A'_\phi P & C'_\phi \bar{\Omega} & H'_\phi \\ (*) & -\bar{\Omega} & 0 & B'_\phi P & 0 & 0 \\ (*) & (*) & -\varepsilon I_{l_1} & E'_\phi P & 0 & 0 \\ (*) & (*) & (*) & -P & 0 & 0 \\ (*) & (*) & (*) & (*) & -\bar{\Omega} & 0 \\ (*) & (*) & (*) & (*) & (*) & -I_{l_2} \end{bmatrix} < 0 \tag{37}$$

where $A_\phi, B_\phi, E_\phi, H_\phi$, are defined in (35), and

$$\begin{aligned} \bar{\Omega} &= diag\left(\Omega_u,\ \Omega_y\right), \\ C_\phi &= \begin{bmatrix} 0 & 0 & -\sigma_u D_\eta D_\xi \bar{C}_y & \sigma_u D_\eta \bar{C}_\xi & \sigma_u C_\eta \\ \sigma_y C & 0 & 0 & 0 & 0 \end{bmatrix} \end{aligned} \tag{38}$$

Moreover, a level of robustness $\delta_\Delta = \varepsilon^{-1/2}$ is guaranteed, where δ_Δ is defined in (4).

Proof: For stability analysis, consider null values for reference signal and external disturbance (i.e, $\bar{y}^T_{ref,k} = 0$ and $\bar{\omega}^T_k = 0$). Then, the forward system $\mathcal{S}$ in (33) can be written as:

$$\bar{\phi}^T_{k+1} = A_\phi \bar{\phi}^T_k + B_\phi \bar{\rho}^T_k + \delta_\Delta E_\phi w^T_{\Delta,k} \tag{39}$$

Consider the Lyapunov function $V_k = \left(\phi^T_k\right)' P \phi^T_k$. Taking into account (39), the forward difference operator $\Delta V_k = V_{k+1} - V_k$ renders:

$$\begin{aligned} \Delta V_k &= \left(\phi^T_{k+1}\right)' P \phi^T_{k+1} - \left(\phi^T_k\right)' P \phi^T_k \\ &= \left(\phi^T_k\right)' \left(A'_\phi P A_\phi - P\right) \phi^T_k + 2\left(\phi^T_k\right)' A'_\phi P B_\phi \bar{\rho}^T_k \\ &+ 2\delta_\Delta \left(\phi^T_k\right)' A'_\phi P E_\phi w^T_{\Delta,k} + \left(\bar{\rho}^T_k\right)' B'_\phi P B_\phi \bar{\rho}^T_k \\ &+ 2\delta_\Delta \left(\bar{\rho}^T_k\right)' B'_\phi P E_\phi w^T_{\Delta,k} + \delta^2_\Delta \left(w^T_{\Delta,k}\right)' E'_\phi P E_\phi w^T_{\Delta,k} \end{aligned} \tag{40}$$

Pre-and post-multiplying (37) by $\text{diag}\big(I, I, \delta_\Delta I, P^{-1}, \bar{\Omega}^{-1}, I\big)$ and further applying Schur Complement in the third and fourth rows and columns, it is

easy to deduce that

$$\begin{bmatrix} \phi_k^T \\ \bar{\rho}_k^T \\ w_{\Delta,k}^T \end{bmatrix}' \begin{bmatrix} A_\phi' P A_\phi - P \\ +C_\phi' \bar{\Omega} C_\phi + H_\phi' H_\phi & A_\phi' P B_\phi & \delta_\Delta A_\phi' P E_\phi \\ (*) & B_\phi' P B_\phi - \bar{\Omega} & \delta_\Delta B_\phi' P E_\phi \\ (*) & (*) & \delta_\Delta^2 E_\phi' P E_\phi - I_{l_1} \end{bmatrix} \begin{bmatrix} \phi_k^T \\ \bar{\rho}_k^T \\ w_{\Delta,k}^T \end{bmatrix} < 0$$

is true $\forall \phi_k^T, \bar{\rho}_k^T, w_{\Delta,k}^T \neq 0$ if and only if (37) holds.

From (7) and (8) it can be seen that:

$$(y_k^T - \tilde{y}_k^T)' \Omega_y (y_k^T - \tilde{y}_k^T) \leq \sigma_y^2 \left(y_k^T\right)' \Omega_y y_k^T + \delta_y \tag{41}$$

Analogously, from (9) and (10), the following inequality is true

$$(u_k^T - \tilde{u}_k^T)' \Omega_u (u_k^T - \tilde{u}_k^T) \leq \sigma_u^2 \left(u_k^T\right)' \Omega_u u_k^T + \delta_u \tag{42}$$

Applying the definition of $\rho_{u,k}^T$, $\rho_{y,k}^T$ in (21), (23) respectively, the above inequalities (42), (41) can be rewritten as:

$$\begin{aligned} \left(\rho_{u,k}^T\right)' \Omega_u \rho_{u,k}^T &\leq \sigma_u^2 \left(u_k^T\right)' \Omega_u u_k^T + \delta_u, \\ \left(\rho_{y,k}^T\right)' \Omega_y \rho_{y,k}^T &\leq \sigma_y^2 \left(y_k^T\right)' \Omega_y y_k^T + \delta_y \end{aligned} \tag{43}$$

The inequalities (43) can be formulated in compact form as:

$$\left(\bar{\rho}_k^T\right)' \bar{\Omega} \bar{\rho}_k^T \leq \left(\bar{y}_{\phi,k}^T\right)' \bar{\Omega} \bar{y}_{\phi,k}^T + \delta \tag{44}$$

where $\bar{\Omega} = diag\left(\Omega_u,\ \Omega_y\right)$, $\delta = \delta_u + \delta_y$ and

$$\bar{y}_{\phi,k}^T = C_\phi \bar{\phi}_k^T \tag{45}$$

where C_ϕ is defined in (38) and $\bar{\phi}_k^T$ is defined in (34). From the definition of Δ_k in (4), it can be deduced that

$$\left(y_{\Delta,k}^T\right)' y_{\Delta,k}^T \leq \left(w_{\Delta,k}^T\right)' w_{\Delta,k}^T \tag{46}$$

By considering $\delta = 0$, the fulfilment of the condition $\bar{J} = \sum_{k=0}^{\infty} \left(\Delta V_k + J_k\right) < 0$ with

$$J_k = \left(\bar{\rho}_k^T\right)' \bar{\Omega} \bar{\rho}_k^T - \left(\bar{y}_{\phi,k}^T\right)' \bar{\Omega} \bar{y}_{\phi,k}^T + \left(y_{\Delta,k}^T\right)' y_{\Delta,k}^T - \left(w_{\Delta,k}^T\right)' w_{\Delta,k}^T \tag{47}$$

implies: (i) the negativeness of the forward difference: $\Delta V_k < 0$ and, (ii) the fulfillment of the inequalities (44) and (46) under zero initial conditions for the augmented state variable $\bar{\phi}_k^T$ in (34). The former condition proves the stability of the closed-loop system, whereas the latter condition proves: (i) the robustness stability under event-triggered condition for some $\sigma_u, \sigma_y > 0$, and (ii) robustness against model uncertainties given by $\left(y_{\Delta,k}^T\right)' y_{\Delta,k}^T \leq \left(w_{\Delta,k}^T\right)' w_{\Delta,k}^T$. Finally, by considering $\delta > 0$, the above condition renders $\bar{J} < \delta$ when the system state is close to the equilibrium point, and $\bar{J} < 0$ otherwise. Hence, the steady-state error remains bounded inside a ball whose radius is proportional to δ. □

Remark 3. *The maximum level of robustness of the closed-loop system* (33) *can be determined by solving the following convex optimization problem:*

$$min\ \varepsilon\ s.t.\ LMI\ (37) \tag{48}$$

where the upper bound for model uncertainties defined in (4) *can be obtained as* $\delta_\Delta = \varepsilon^{-1/2}$.

Remark 4. *The robust stability algorithm given in Theorem 1 is based on the quadratic Lyapunov function* $V_k = \left(\phi_k^T\right)' P \phi_k^T$. *The advantage of this choice is that conservatism is reduced to the greatest extent since no loss of generality is introduced in the Lyapunov function. Nevertheless, the drawback is that computational complexity is proportional to the number of consecutive packet dropouts* h, *as can be deduced from the number of decision variables (NoV) and size of LMI* (37), *which are respectively* $\frac{1}{2}\bar{n}\left(\bar{n}+1\right)+\frac{1}{2}m\left(m+1\right)+\frac{1}{2}q\left(q+1\right)+1$ *and* $2\bar{n}+m+q+l_1+l_2$, *where* $\bar{n} = n+hN(m+n)+Nn_\xi+n_\eta$.

5. Application to a UGV

In this section, the control solution proposed in this work is applied to a two-wheel UGV tracking control. In order to carry out this kind of control, the reference generator depicted in Fig. 1 needs to include a path tracking algorithm. In this case, Pure Pursuit is chosen (introduced in Section 5.1). The UGV and the main application data are presented in Section 5.3, where the closed-loop stability analysis is also performed. Simulation results, together with their experimental validation, are shown in Section 5.4, where some cost indexes (presented in section 5.2) are used to better quantify the benefits of the control approach, compared to other options.

5.1. Pure Pursuit path tracking algorithm

The Pure Pursuit path tracking algorithm is in charge of computing the velocity and turning conditions so that the UGV can follow a prescribed trajectory [29]. More concretely, by means of this algorithm, and using an odometry technique, the UGV is able to infer its current position from the prescribed kinematic reference $(X_{ref}, Y_{ref}, \theta_{ref})_k^{NT}$ and the plant output estimate generated by the TVDRKF at period NT, $(\hat{w}_r, \hat{w}_l)_k^{NT} \equiv \hat{y}_k^{NT}$, being $(\hat{w}_r, \hat{w}_l)_k^{NT}$ the rotational velocity for the right and left wheel motors, respectively. Then, with the aim of properly reaching the next point of the desired trajectory, the algorithm generates the dynamic reference based on the rotational velocity for both wheels, i.e., $(w_{r,ref}, w_{l,ref})_k^{NT} \equiv y_{ref,k}^{NT}$.

The UGV path tracking is composed of a set of h future dynamic references, $\{y_{ref,k}^{NT}, y_{ref,k+1}^{NT}, \ldots, y_{ref,k+h}^{NT}\}$. In order to establish these references, the reference generator provides in advance the Pure Pursuit algorithm with the sequence of h-step ahead kinematic references:

$$\{(X_{ref}, Y_{ref}, \theta_{ref})_k^{NT}, (X_{ref}, Y_{ref}, \theta_{ref})_{k+1}^{NT}, \ldots, (X_{ref}, Y_{ref}, \theta_{ref})_{k+h}^{NT}\}$$

The main steps of the Pure Pursuit algorithm are (more details can be found in [1]):

1. Calculation of rotational and linear velocities (ω_k^{NT} and v_k^{NT}, respectively) from $\hat{w}_{r,k}^{NT}$ and $\hat{w}_{l,k}^{NT}$:

$$v_{r,k}^{NT} = \hat{w}_{r,k}^{NT} r \tag{49}$$
$$v_{l,k}^{NT} = \hat{w}_{l,k}^{NT} r \tag{50}$$
$$v_k^{NT} = \frac{v_{r,k}^{NT} + v_{l,k}^{NT}}{2} \tag{51}$$
$$\omega_k^{NT} = \frac{v_{r,k}^{NT} - v_{l,k}^{NT}}{l} \tag{52}$$

   being r the wheel radius, and l the distance between the two wheels.

2. UGV position and orientation computation in the time period NT:

$$X_k^{NT} = X_{k-1}^{NT} + v_k^{NT} NT \cos(\theta_{k-1}^{NT} + \omega_k^{NT} NT) \tag{53}$$
$$Y_k^{NT} = Y_{k-1}^{NT} + v_k^{NT} NT \sin(\theta_{k-1}^{NT} + \omega_k^{NT} NT) \tag{54}$$
$$\theta_k^{NT} = \theta_{k-1}^{NT} + \omega_k^{NT} NT \tag{55}$$

   for $k \in \mathbb{N}_{\geq 1}$, where $(X, Y, \theta)_0^{NT}$ is the initial position and orientation.

3. Generation of the future reference for the UGV, $(X_{ref}, Y_{ref})_k^{NT}$, from the Look Ahead Distance (LAD) and the prescribed kinematic reference.
4. Computation of control law $\bar{k}$ at period NT:

$$\bar{k} = 2\frac{(Y_{ref,k}^{NT} - Y_k^{NT})\cos(\theta_k^{NT}) - (X_{ref,k}^{NT} - X_k^{NT})\sin(\theta_k^{NT})}{(X_{ref,k}^{NT} - X_k^{NT})^2 + (Y_{ref,k}^{NT} - Y_k^{NT})^2} \tag{56}$$

As a result, and given a desired linear velocity $v_{ref,k}^{NT}$, the rotational velocity reference $\omega_{ref,k}^{NT}$ and the dynamic references $(w_{r,ref}, w_{l,ref})_k^{NT}$ are calculated as follows:

$$\omega_{ref,k}^{NT} = v_{ref,k}^{NT}\bar{k} \tag{57}$$

$$(w_{r,ref})_k^{NT} = \frac{v_{ref,k}^{NT} + \omega_{ref,k}^{NT} b}{r} \tag{58}$$

$$(w_{l,ref})_k^{NT} = \frac{v_{ref,k}^{NT} - \omega_{ref,k}^{NT} b}{r} \tag{59}$$

where b is half of the distance between the two wheels.

The algorithm is repeated for the h-step ahead predictions. Figure 4 illustrates the different algorithm stages.

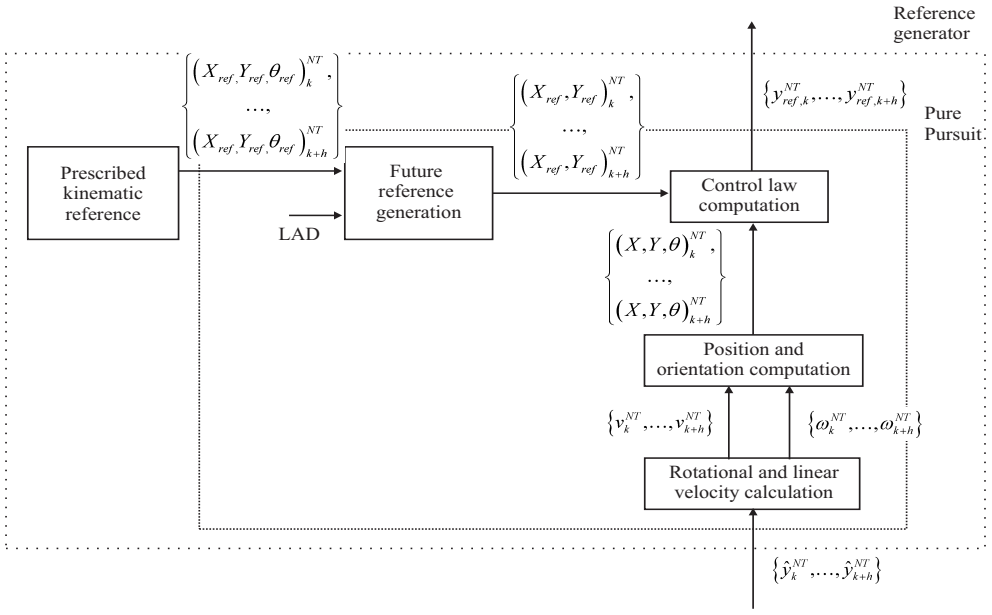

Figure 4: Structure of the reference generator, including Pure Pursuit

5.2. Cost indexes for control performance and resource usage

In this section, some cost indexes are presented to better quantify control performance and resource usage. Some comparisons will be carried out in Section 5.4, focusing on revealing the benefits of the proposed energy-efficient event-triggered control solution versus the conventional time-triggered one.

Three cost indexes will be used to analyze control performance (see [1] for details):

- J_1, which is based on the ℓ_2-norm:

$$J_1 = \sum_{k=1}^{l} \min_{1 \le k' \le l} \sqrt{(X_k^{NT} - X_{ref,k'}^{NT})^2 + (Y_k^{NT} - Y_{ref,k'}^{NT})^2} \tag{60}$$

  where l is the number of iterations to reach the final destination, and $(X_{ref}, Y_{ref})_{k'}^{NT}$ is the nearest kinematic position reference to the current UGV position.

- J_2, which is based on the ℓ_∞-norm:

$$J_2 = \max_{1 \le k \le l} \left\{ \min_{1 \le k' \le l} \sqrt{(X_k^{NT} - X_{ref,k'}^{NT})^2 + (Y_k^{NT} - Y_{ref,k'}^{NT})^2} \right\} \tag{61}$$

- J_3, which measures the total amount of time (in seconds) required to reach the final destination:

$$J_3 = lNT \tag{62}$$

As in [1], to analyze resource saving, the cost index J_4 measures (in %) the reduction of the number of packets transmitted by the proposed solution, NoT_{EEC}, versus the conventional one, NoT_{TTC}:

$$J_4 = \frac{NoT_{\mathrm{EEC}}}{NoT_{\mathrm{TTC}}} \cdot 100\%. \tag{63}$$

5.3. Robust stability analysis

Consider a plant system consisting in the two-wheel UGV. The system model for both wheel motors is described by means of the following transfer function [1]:

$$G_p(s) = \frac{0.1276}{0.1235s + 1} \tag{64}$$

where the output is expressed in rad/s, and the input in V. The disturbance model is given by the exogenous system with system matrices:

$$A_d = \begin{bmatrix} 0.9993 & 0.09994 \\ -0.0142 & 0.9985 \end{bmatrix},\ B_d = \begin{bmatrix} 3.769 \cdot 10^{-5} \\ 0.7535 \cdot 10^{-3} \end{bmatrix},\ C_d = \begin{bmatrix} 0 & 10^5 \end{bmatrix} \quad (65)$$

Previous off-line experiences on the NCS framework lead to consider a maximum time delay τ_{max} slightly less than 200ms. Then, as commented in Section 2 (Assumption 1), the sensor period is chosen as NT=0.2s in order to ensure no packet disorder. Choosing $N = 2$ allows the UGV to accurately track the path, as it will be shown in Section 5.4.

In this simulation, let us assume the packet dropout probability as p_{sc}=0.1 and p_{ca}=0.3 in (2).

Now, consider the continuous-time PID controller

$$u(t) = K_p \left[e(t) + \frac{1}{T_i} \int_0^t e(\tau) d\tau \right]$$

where $K_p = 6$ and $T_i = 0.12$. The discretization of the above controller at period $T = 0.1s$ and $NT = 0.2s$ yields respectively

$$G_r^T(z) = \frac{6z - 1}{z - 1} \quad (66)$$

$$G_r^{NT}(z^N) = \frac{6z + 4}{z - 1} \quad (67)$$

Also, the ZOH-discretized plant (64) with sampling period T leads to $G_p(z) = \frac{0.07082}{z-0.445}$, which can be expressed in state-space model as (1) with matrices:

$$A_p = 0.4450, \quad B_p = 0.2500, \quad C_p = 0.2833 \quad (68)$$

For robust performance analysis, time-varying model uncertainties $\Delta_{A,k},\ \Delta_{B,k}$ on the form (4) are considered with $E_p = 1$, $H_{p,A} = 1$, $H_{p,B} = 1$, where the scalar δ_Δ will be later used as robust performance index.

The dual-rate controller with $N = 2$ is obtained by means of (19) and (20), leading to

$$G_1^{NT}(z^N) = \frac{z^2 - 0.4734z + 0.05731}{z^2 - 1.191z + 0.1914} \quad (69)$$

$$G_2^T(z) = \frac{6.576z^2 - 5.78z + 1.27}{z^2 - 0.9578z + 0.2394} \quad (70)$$

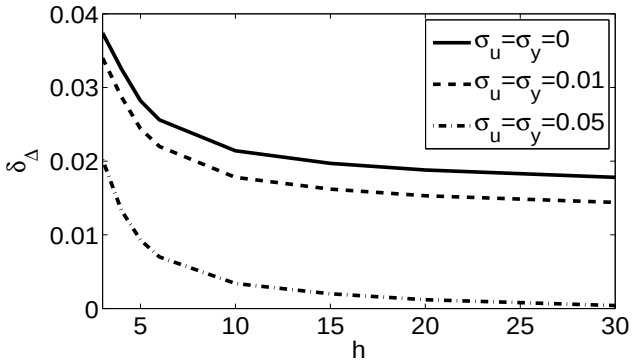

Figure 5: Robust index δ_Δ with respect to the maximum number of consecutive measurement packet dropouts h

The state-space matrices of the slow-rate and fast-rate controllers are respectively:

$$A_\xi = \begin{bmatrix} 1.1914 & -0.3829 \\ 0.5000 & 0 \end{bmatrix},\ B_\xi = \begin{bmatrix} 1 \\ 0 \end{bmatrix}, \tag{71}$$
$$C_\xi = \begin{bmatrix} 0.7180 & -0.2683 \end{bmatrix},\ D_\xi = 1,$$

$$A_\eta = \begin{bmatrix} 0.9758 & -0.4788 \\ 0.5000 & 0 \end{bmatrix},\ B_\eta = \begin{bmatrix} 1 \\ 0 \end{bmatrix},$$
$$C_\eta = \begin{bmatrix} 0.6367 & -0.6086 \end{bmatrix},\ D_\eta = 6.5759$$

The parameter of the Kalman filter observed in simulation and experiments ranges between $K(\bar{N}) = \begin{bmatrix} 14.1188 & 0 & 0.0001 \end{bmatrix}$ for $\bar{N} = N$ and $K(\bar{N}) = \begin{bmatrix} 14.1202 & 0 & 0.0001 \end{bmatrix}$ for $\bar{N} \geq 6N$. For the robust performance analysis, we have taken the mean value $K(\bar{N}) = \begin{bmatrix} 14.1195 & 0 & 0.0001 \end{bmatrix}$ since time variations in $K(\bar{N})$ can be considered negligible.

Fig. 5 depicts the closed-loop robustness margin δ_Δ in (4) obtained by solving the convex optimization problem described in Remark 3 and Theorem 1. The robust performance has been evaluated as a function of the maximum number of consecutive packet dropouts h under three different choices of event-triggered parameters σ_u and σ_y with the same value for the sake of simplicity. On one hand, it is interesting to see that robustness decreases more slowly for larger values of h, which reveals that the designed NCS keeps a good robust performance even for large number of consecutive

packet dropouts. On the other hand, it can be appreciated that the robustness decreases as long as the event-triggered parameters σ_u, σ_y are higher, showing an existing trade-off between robust performance and bandwidth reduction. The event-triggered parameters Ω_u, Ω_y in Theorem 1 have been chosen as $\Omega_u = \Omega_y = 1$ since the input and output dimensions are equal to 1, and therefore these parameters have no influence in robust performance by properly scaling σ_u, σ_y.

For the experimental setup, we have proposed the event-triggered parameters $\sigma_u = \sigma_y = 0$, $\Omega_u = \Omega_y = 1$, $\delta_y = 0.01$ and $\delta_u = 0.5$. The values of σ_u, σ_y have been chosen to enhance the closed-loop robust performance following Remark 3. As a result, the parameter $\varepsilon = 946.7456$ is obtained, which corresponds to a robustness margin $\delta_\Delta = 0.0325$. The values of δ_u, δ_y has been chosen to achieve some benefits in terms of reduction of bandwidth usage and energy consumption with a reasonable steady-state error, in light of the simulation and experimental results. The maximum number of consecutive packet dropouts will be set as $h = 4$, and the reference to be followed will include a sequence of four right angles.

5.4. Simulation results and experimental validation

In this section, the main advantages of the energy-efficient event-triggered control solution compared to different options for the time-triggered approach will be shown. The study will be focused on the trade-off between resource usage and control properties.

Simulation results will be experimentally validated by means of a test-bed platform, which is based on a two-wheel Lego Mindstorms EV3 robot equipped with a wifi-dongle to send and receive data-packages. A picture of the robot is shown in Figure 6.

Figure 6: The Lego Mindstorms EV3 robot used in the implementation

The proposed structure consists of two parts: i) at the remote side, a stationary, powerful computer is used to calculate all the set of control actions; ii) at the local side, the UGV, equipped with encoders and actuators, is employed. The control application is made in Matlab/Simulink®. The code programmed at the local side is kept as simple as possible because of the limited hardware capabilities of the UGV, and hence, it mainly includes User Datagram Protocol (UDP) send and receive blocks to wirelessly communicate with the remote side. The remote side includes these communication blocks as well, and the ones required to implement the control strategy. The model can be switched between experimental mode and simulation mode by changing the UDP blocks to a block representing the transfer function of each motor.

The following results (Figures 7-12) are obtained by running both working modes for different scenarios. In each figure, the simulated results are shown at the left hand, while the experimental validation is depicted at the right hand.

Let us start the comparison considering a time-triggered single-rate control scenario with neither noise nor disturbance, and neither time-varying delays nor packet dropouts. Under these conditions, the UGV path tracking behavior achieved by the controller designed at period NT=0.2s in (67) (depicted in Figure 8) is compared with the behavior obtained by the controller

designed at period T=0.1s in (66) (shown in Figure 7). The comparison illustrates a considerable performance worsening for the former case.

Let us consider the performance reached at period T as the nominal, desired one. Taking into account the dual-rate controller in (69)-(70), which injects control actions at period T but measures system outputs at period NT, the time-triggered dual-rate control system is able to maintain a satisfactory control performance, very similar to the nominal one (as shown in Figure 9). Nevertheless, whether both time-varying delays and packet dropouts are included in the NCS, the performance is clearly worsened, becoming unstable (see in Figure 10).

Note also that the control system performance is clearly improved (as illustrated in Figure 11) by incorporating the TVDRKF into the time-triggered dual-rate control system (assuming delays and dropouts), together with the packet-based control. It can be appreciated that the obtained performance is very similar to the nominal one, despite the presence of measurement noise and external disturbances.

Finally, event-triggered conditions are added to the NCS, and then, the system becomes a periodic event-triggered dual-rate control system. The performance obtained is similar to that reached by the nominal time-triggered version of the system (see in Figure 12), but now a clear reduction of the number of transmitted packets is achieved, which leads to reducing resource usage (bandwidth, energy). This aspect will be analyzed in detail in Table 1.

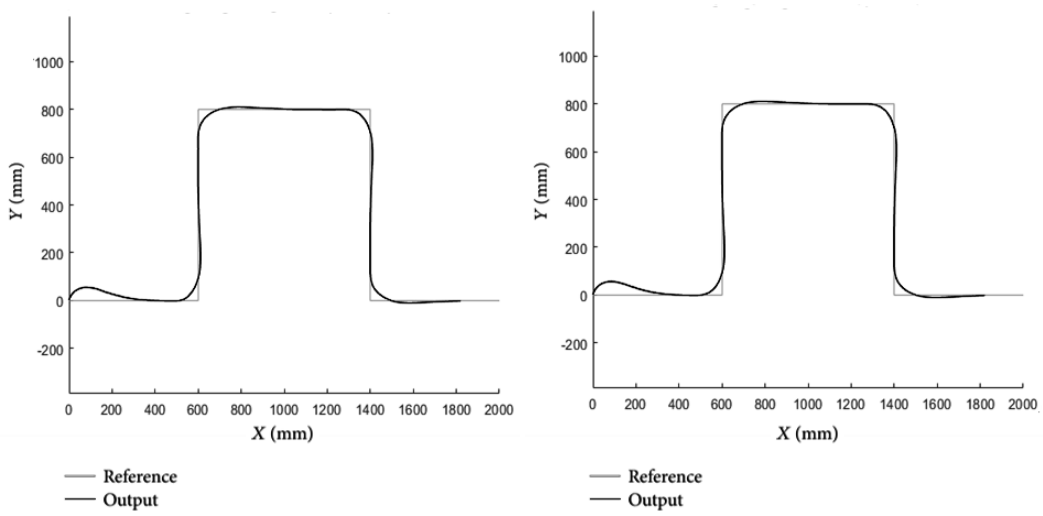

(a) Simulated result (b) Experimental result

Figure 7: Comparison for the time-triggered single-rate T=0.1s case (nominal performance; scenario b)

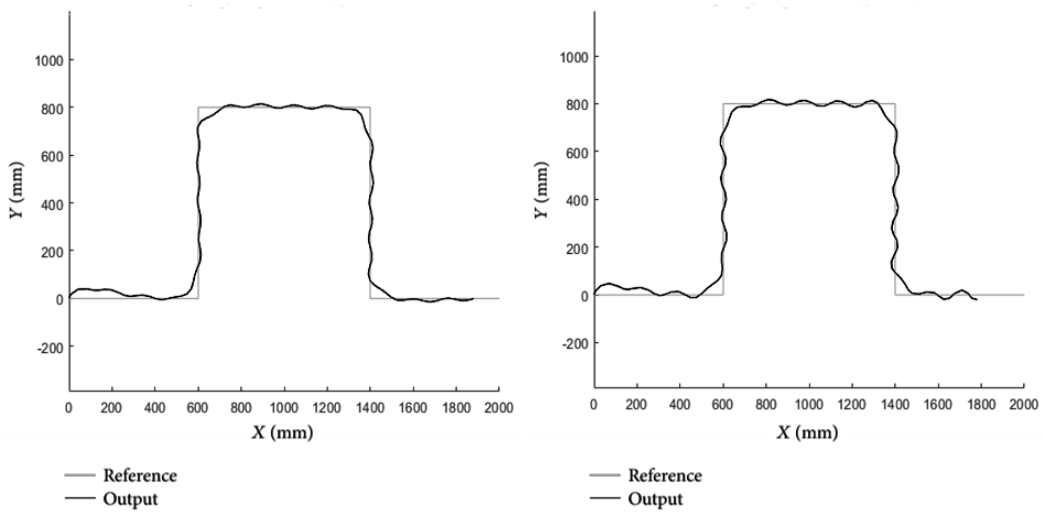

(a) Simulated result (b) Experimental result

Figure 8: Comparison for the time-triggered single-rate NT=0.2s case (scenario a)

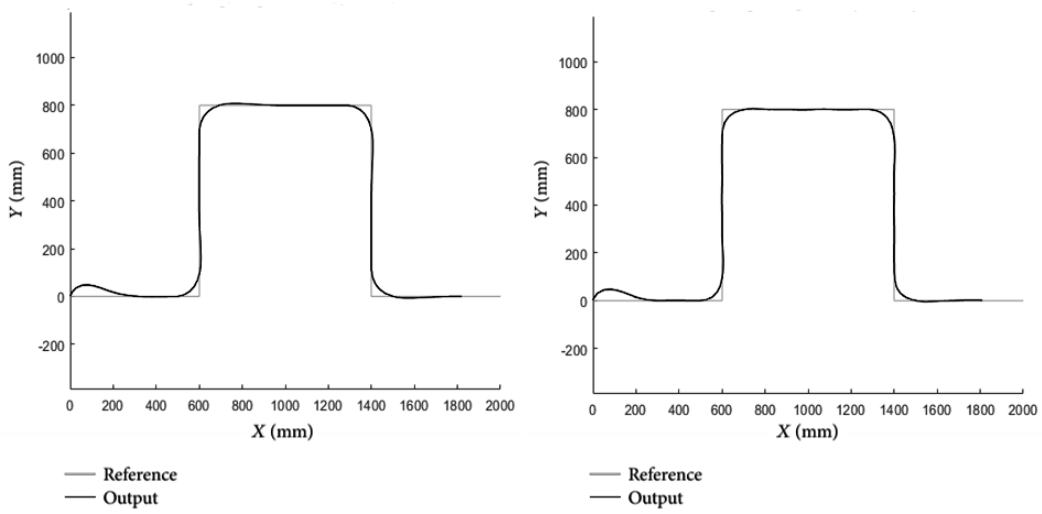

(a) Simulated result (b) Experimental result

Figure 9: Comparison for the time-triggered dual-rate NT=0.2s and T=0.1s case (scenario c)

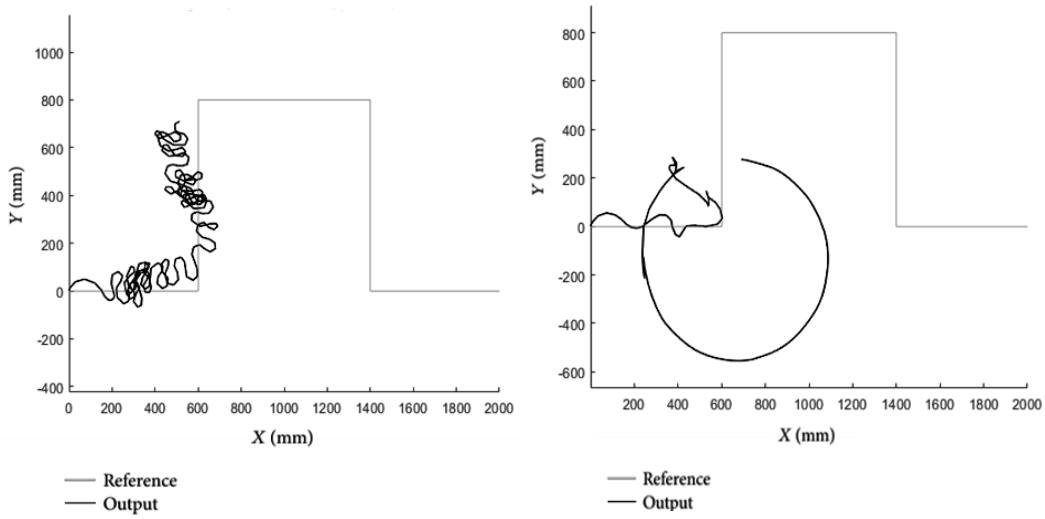

(a) Simulated result (b) Experimental result

Figure 10: Comparison for the time-triggered dual-rate case, with delays and dropouts

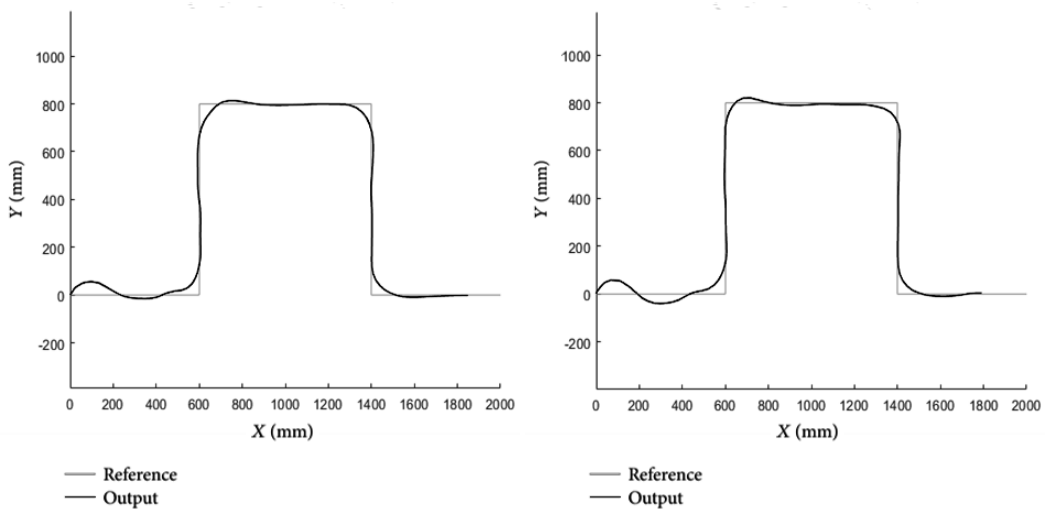

(a) Simulated result (b) Experimental result

Figure 11: Comparison for the time-triggered dual-rate case, with TVDRKF and packet-based control, including delays, dropouts, noise and disturbances (scenario d)

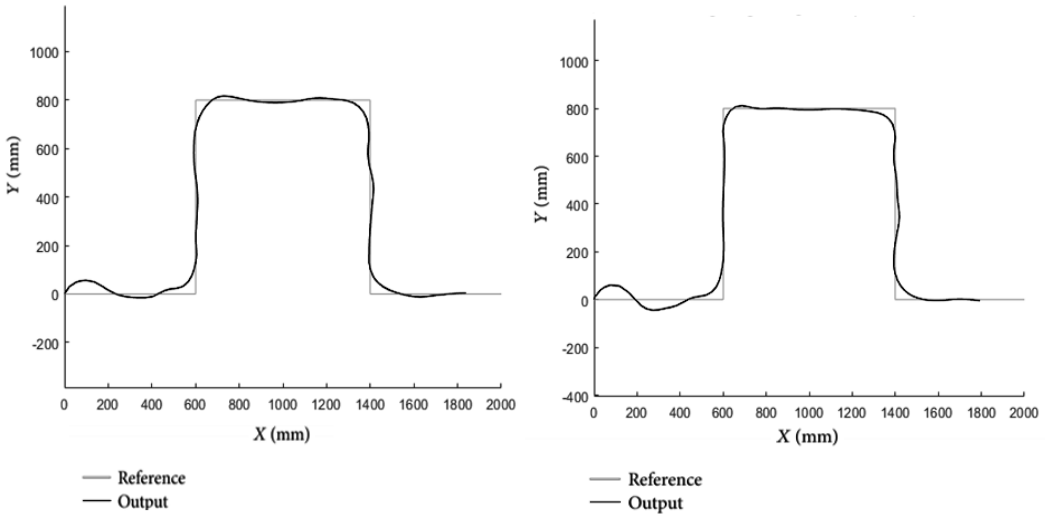

(a) Simulated result (b) Experimental result

Figure 12: Comparison for the periodic event-triggered dual-rate case, with TVDRKF and packet-based control, including delays, dropouts, noise and disturbances (scenario e)

As shown in Figures 7-12, the experimental results accurately validate

the simulations. For this reason, the cost indexes presented in Section 5.2 will be directly evaluated from the experimentation. As the indexes may be negatively affected by the initialization part of the path, they will be calculated starting from iteration $k = 20$. Table 1 summarizes the values obtained for the five different stable cases previously shown, that is:

- a: time-triggered single-rate control scenario at period NT (in Figure 8).
- b: time-triggered single-rate control scenario at period T (in Figure 7).
- c: time-triggered dual-rate control scenario (in Figure 9).
- d: time-triggered dual-rate control scenario, adding TVDRKF, and packet-based control, including dropouts, delays, disturbances and noise (in Figure 11).
- e: periodic event-triggered dual-rate control scenario, with TVDRKF, and packet-based control, including dropouts, delays, disturbances and noise (in Figure 12).

	a	b	c	d	e
J_1	1328.3	1078.9	1085.0	1160.2	1189.9
J_2	47.13	38.30	38.88	39.62	40.98
J_3	22.4	22.0	22.0	22.0	22.0
J_4	50%	100%	50%	50%	37.1%

Table 1: Cost indexes from the experimentation

The underlying conclusions of Table 1 are:

- The desired nominal performance (scenario b) presents the best (lowest) values for the cost indexes related to control performance, that is, J_1, J_2, J_3. The obtained values have been considered as the reference ones to carry out the comparison on control performance.
- Considerations for J_1: the single-rate case at period NT (scenario a) shows the worst J_1, since the desired trajectory is inaccurately followed by the UGV. The dual-rate case for scenario c shows a similar J_1 than the nominal scenario b. However, the dual-rate case for scenarios d and

e worsen the index J_1 around 7% and 10%, respectively, compared to the nominal performance.

- Considerations for J_2: again, scenario a (single-rate at NT) presents the worst value, being the dual-rate scenario c very similar to the nominal scenario b. The dual-rate scenarios d and e worsen the index J_2 around 3% and 7%, respectively, compared to the nominal performance.

- Considerations for J_3: this cost index presents the same value for the dual-rate cases c, d, and e as for the nominal case b, being 1% worse for the single-rate scenario a (at NT).

- Finally, to carry out the comparison on resource saving, J_4 will be analyzed. It presents the worst case in scenario b (single-rate at T), being 50% reduced by scenarios a, c and d because of sampling the network twice slower (at NT, with $N = 2$). The periodic event-triggered scenario e reaches the best value for index J_4 with around 63% of reduction, compared to the scenario b.

As a summary, the periodic event-triggered dual-rate control scenario, with TVDRKF and packet-based control is able to significantly reduce resource usage (bandwidth, energy) with almost 63% of reduction, while having a performance worsening of only up to 10%, with regards to the nominal time-triggered case. This is in spite of existing dropouts, delays, disturbances and noise acting on the system.

6. Conclusions

This paper has addressed a formal analysis of the closed-loop stability and robust performance of an energy-efficient control in the framework of NCS, consisting in an event-triggered dual-rate control with a TVDRKF applied to a UGV. Different aspects, such as packet dropouts, time-varying model mismatches, disturbance rejection and event-triggered thresholds have been taken into account in the stability analysis. It has been illustrated that the robust performance is not significantly affected by the maximum number of consecutive packet dropouts in a wide range. In addition, the proposed control strategy has been experimentally validated by tracking the 2D position of a UGV in a wireless network. Despite existing typical network problems such as time-varying delays and packet dropouts, and considering

disturbance and measurement noise, the control solution is able to achieve a satisfactory performance, while considerably reducing resource usage.

Acknowledgement

This research was funded in part by grant by projects PGC2018-098719-B-I00 (MCIU/ AEI/ FEDER, UE), and RTI2018-096590-B-I00 (MCIU/ AEI/ FEDER, UE), and by European Commission as part of Project H2020-SEC-2016-2017 - Topic: SEC-20-BES-2016 - Id: 740736 - "C2 Advanced Multi-domain Environment and Live Observation Technologies" (CAMELOT). Part WP5 supported by Tekever ASDS, Thales Research and Technology, Viasat Antenna Systems, Universitat Politècnica de València, Fundação da Faculdade de Ciências da Universidade de Lisboa, Ministério da Defensa Nacional - Marinha Portuguesa, Ministério da Administração Interna Guarda Nacional Republicana.

References

[1] J. Alcaina, Á. Cuenca, J. Salt, M. Zheng, and M. Tomizuka. Energy-efficient control for an unmanned ground vehicle in a wireless sensor network. *Journal of Sensors*, 2019:Article ID 7085915, 2019.

[2] Y. S. Andrade, R. K. Mansano, E. P. Godoy, and A. J. Porto. Evaluation of aperiodic control for energy saving in wireless networked control systems. In *2016 12th IEEE International Conference on Industry Applications (INDUSCON)*, pages 1–7. IEEE, 2016.

[3] J.-C. Bolot. End-to-end packet delay and loss behavior in the internet. In *ACM SIGCOMM Computer Communication Review*, volume 23, pages 289–298. ACM, 1993.

[4] S. Boyd, L. El Ghaoui, E. Feron, and V. Balakrishnan. *Linear matrix inequalities in system and control theory*, volume 15. SIAM, 1994.

[5] A. Cervin, D. Henriksson, B. Lincoln, J. Eker, and K.-E. Arzen. How does control timing affect performance? Analysis and simulation of timing using Jitterbug and TrueTime. *IEEE Control Systems*, 23(3):16–30, 2003.

[6] M. B. Cloosterman, N. Van de Wouw, W. Heemels, and H. Nijmeijer. Stability of networked control systems with uncertain time-varying delays. *IEEE Transactions on Automatic Control*, 54(7):1575–1580, 2009.

[7] A. Cuenca, J. Alcaina, J. Salt, V. Casanova, and R. Pizá. A packet-based dual-rate PID control strategy for a slow-rate sensing Networked Control System. *ISA Transactions*, 76:155–166, 2018.

[8] A. Cuenca, D. J. Antunes, A. Castillo, P. García, B. A. Khashooei, and W. Heemels. Periodic event-triggered sampling and dual-rate control for a wireless networked control system with applications to UAVs. *IEEE Transactions on Industrial Electronics*, 66(4):3157–3166, 2018.

[9] Á. Cuenca, M. Zheng, M. Tomizuka, and S. Sánchez. Non-uniform multi-rate estimator based periodic event-triggered control for resource saving. *Information Sciences*, 459:86–102, 2018.

[10] S. Ding, X. Xie, and Y. Liu. Event-triggered static/dynamic feedback control for discrete-time linear systems. *Information Sciences*, 524:33–45, 2020.

[11] V. S. Dolk, J. Ploeg, and W. M. H. Heemels. Event-triggered control for string-stable vehicle platooning. *IEEE Transactions on Intelligent Transportation Systems*, 18(12):3486–3500, 2017.

[12] D. Dolz, I. Peñarrocha, and R. Sanchis. Networked gain-scheduled fault diagnosis under control input dropouts without data delivery acknowledgment. *International Journal of Robust and Nonlinear Control*, 26(4): 737–758, 2016.

[13] A. González. A weighted distributed predictor-feedback control synthesis for interconnected time delay systems. *Information Sciences*, 543: 367–381, 2021.

[14] A. Gonzalez, V. Balaguer, P. Garcia, and A. Cuenca. Gain-scheduled predictive extended state observer for time-varying delays systems with mismatched disturbances. *ISA Transactions*, 84:206–213, 2019.

[15] A. González, A. Cuenca, V. Balaguer, and P. García. Event-triggered predictor-based control with gain-scheduling and extended state observer for networked control systems. *Information Sciences*, 491:90–108, 2019.

[16] L. Guo and W.-H. Chen. Disturbance attenuation and rejection for systems with nonlinearity via dobc approach. *International Journal of Robust and Nonlinear Control: IFAC-Affiliated Journal*, 15(3):109–125, 2005.

[17] L. Guo, H. Yu, and F. Hao. Event-triggered control for stochastic networked control systems against denial-of-service attacks. *Information Sciences*, 527:51–69, 2020.

[18] Q.-L. Han and K. Gu. On robust stability of time-delay systems with norm-bounded uncertainty. *IEEE Transactions on Automatic Control*, 46(9):1426–1431, 2001.

[19] Z. Han, N. Xu, H. Chen, Y. Huang, and B. Zhao. Energy-efficient control of electric vehicles based on linear quadratic regulator and phase plane analysis. *Applied Energy*, 213:639–657, 2018.

[20] S. Hao, T. Liu, and B. Zhou. Output feedback anti-disturbance control of input-delayed systems with time-varying uncertainties. *Automatica*, 104:8–16, 2019.

[21] W. H. Heemels, M. Donkers, and A. R. Teel. Periodic event-triggered control for linear systems. *IEEE Transactions on Automatic Control*, 58 (4):847–861, 2012.

[22] B. A. Khashooei, B. van Eekelen, D. J. Antunes, and W. M. H. Heemels. Suboptimal event-triggered control over unreliable communication links with experimental validation. In *2017 3rd International Conference on Event-Based Control, Communication and Signal Processing (EBCCSP)*, pages 1–6. IEEE, 2017.

[23] P. Kühne, F. Pöschke, and H. Schulte. Fault estimation and fault-tolerant control of the FAST NREL 5-MW reference wind turbine using a proportional multi-integral observer. *International Journal of Adaptive Control and Signal Processing*, 32(4):568–585, 2018.

[24] D. Li, S. L. Shah, and T. Chen. Analysis of dual-rate inferential control systems. *Automatica*, 38(6):1053–1059, 2002.

[25] H. Li and Y. Shi. Network-based predictive control for constrained nonlinear systems with two-channel packet dropouts. *IEEE Transactions on Industrial Electronics*, 61(3):1574–1582, 2014.

[26] T. Li, T. Wang, J. Zhai, and S. Fei. Event-triggered observer-based robust H_∞ control for networked control systems with unknown disturbance. *International Journal of Robust and Nonlinear Control*, 30(7): 2671–2688, 2020.

[27] A. Liu, W. A. Zhang, L. Yu, S. Liu, and M. Z. Chen. New results on stabilization of networked control systems with packet disordering. *Automatica*, 52:255–259, 2015.

[28] A. Liu, W. A. Zhang, B. Chen, and L. Yu. Networked filtering with markov transmission delays and packet disordering. *IET Control Theory & Applications*, 12(5):687–693, 2017.

[29] M. Lundgren. Path tracking and obstacle avoidance for a miniature robot. *Umeå University, Umeå, Master Thesis*, 2003.

[30] Y. Luo, X. Xiao, J. Cao, A. Li, and G. Lin. Event-triggered guaranteed cost consensus control for second-order multi-agent systems based on observers. *Information Sciences*, 546:283–297, 2021.

[31] B. Park, J. Nah, J.-Y. Choi, I.-J. Yoon, and P. Park. Robust wireless sensor and actuator networks for networked control systems. *Sensors*, 19(7):1535, 2019.

[32] I. Peñarrocha, R. Sanchis, and J. A. Romero. State estimator for multisensor systems with irregular sampling and time-varying delays. *International Journal of Systems Science*, 43(8):1441–1453, 2012.

[33] V. Raghunathan, C. Schurgers, S. Park, and M. B. Srivastava. Energy-aware wireless microsensor networks. *IEEE Signal Processing Magazine*, 19(2):40–50, 2002.

[34] A. Sala, A. Cuenca, and J. Salt. A retunable PID multi-rate controller for a networked control system. *Information Sciences*, 179(14):2390–2402, 2009.

[35] J. Salt and P. Albertos. Model-Based Multirate Controllers Design. *IEEE Transactions on Control Systems Technologies*, 13(6):988–997, Nov. 2005.

[36] D. Shah, A. Mehta, K. Patel, and A. Bartoszewicz. Event-triggered discrete higher-order smc for networked control system having network irregularities. *IEEE Transactions on Industrial Informatics*, 16(11):6837–6847, 2020.

[37] J. M. Simkoff, F. Lejarza, M. T. Kelley, C. Tsay, and M. Baldea. Process control and energy efficiency. *Annual Review of Chemical and Biomolecular Engineering*, 11:423–445, 2020.

[38] D. Simon. *Optimal state estimation: Kalman, H_∞, and nonlinear approaches*. John Wiley & Sons, 2006.

[39] J. Širokỳ, F. Oldewurtel, J. Cigler, and S. Prívara. Experimental analysis of model predictive control for an energy efficient building heating system. *Applied Energy*, 88(9):3079–3087, 2011.

[40] Y. S. Suh. Stability and stabilization of nonuniform sampling systems. *Automatica*, 44(12):3222–3226, 2008.

[41] S. Trimpe and R. D'Andrea. Event-based state estimation with variance-based triggering. *IEEE Transactions on Automatic Control*, 59(12): 3266–3281, 2014.

[42] N. S. Tripathy, M. Chamanbaz, and R. Bouffanais. Robust stabilization of resource limited networked control systems under denial-of-service attack. In *2019 IEEE 58th Conference on Decision and Control (CDC)*, pages 7683–7689. IEEE, 2019.

[43] N. S. Tripathy, I. N. Kar, M. Chamanbaz, and R. Bouffanais. Robust stabilization of a class of nonlinear systems via aperiodic sensing and actuation. *IEEE Access*, 8:157403–157417, 2020.

[44] X. Xia and J. Zhang. Energy efficiency and control systems–from a POET perspective. *IFAC Proceedings Volumes*, 43(1):255–260, 2010.

[45] X. Xia and L. Zhang. Industrial energy systems in view of energy efficiency and operation control. *Annual Reviews in Control*, 42:299–308, 2016.

[46] J. Zhang, H. Zhang, S. Sun, and Z. Gao. Leader-follower consensus control for linear multi-agent systems by fully distributed edge-event-triggered adaptive strategies. *Information Sciences*, 555:314–338, 2021.

[47] X.-M. Zhang, Q.-L. Han, X. Ge, D. Ding, L. Ding, D. Yue, and C. Peng. Networked control systems: a survey of trends and techniques. *IEEE/CAA Journal of Automatica Sinica*, 7(1):1–17, 2019.

[48] M. Zheng, X. Chen, and M. Tomizuka. Extended state observer with phase compensation to estimate and suppress high-frequency disturbances. In *American Control Conf. (ACC)*, pages 3521–3526. IEEE, 2016.

[49] M. Zheng, L. Sun, and M. Tomizuka. Multi-rate observer based sliding mode control with frequency shaping for vibration suppression beyond Nyquist frequency. *IFAC-PapersOnLine*, 49(21):13–18, 2016.

[50] T. Zou, S. Lin, Q. Feng, and Y. Chen. Energy-efficient control with harvesting predictions for solar-powered wireless sensor networks. *Sensors*, 16(1):53, 2016.